

# Urban Running Activity Detected Using a Seismic Sensor during COVID-19 Pandemic

Yumin Zhao<sup>1</sup> , Yunyue Elita Li<sup>\*1,2</sup>, Enhedelihai Nilot<sup>1</sup> , and Gang Fang<sup>1</sup> 

## Abstract

Human foot traffic in urban environments provides essential information for city planners to manage the urban resources and urban residents to plan their activities. Compared to camera or mobile-based solutions, seismic sensors detect human footstep signals with fewer privacy concerns. However, seismic sensors often record signals generated from multiple sources, particularly in an urban outdoor environment. In this article, we monitor people's running activities during COVID-19 pandemic with a seismic sensor in a park in Singapore. We compare the spectra of natural and urban events in the recorded seismic data. For each 3 s seismic data, we define hierarchical screening criteria to identify footsteps based on the spectrum of the signal and its envelope. We derive the cadence of each runner by detecting the primary frequency of the footstep signals. The resulting algorithm achieves higher accuracy and higher temporal resolution for weak and overlapping signals compared to existing methods. Runner statistics based on four-month long seismic data show that urban running activities have clear daily and weekly cycles. Lockdown measures to mitigate COVID-19 pandemic promoted running activities, particularly over the weekends. Cadence statistics show that morning runners have higher cadence on average.

**Cite this article as** Zhao, Y., Y. E. Li, E. Nilot, and G. Fang (2021). Urban Running Activity Detected Using a Seismic Sensor during COVID-19 Pandemic, *Seismol. Res. Lett.* **XX**, 1–12, doi: [10.1785/0220210147](https://doi.org/10.1785/0220210147).

## Supplemental Material

## Introduction

COVID-19 pandemic has a significant impact on the world's economy (e.g., Baldwin and Weder, 2020; Bonaccorsi *et al.*, 2020; Maliszewska *et al.*, 2020), environments (e.g., Baldasano, 2020; Sicard *et al.*, 2020; Zambrano-Monserrate *et al.*, 2020), and human activities (e.g., Lecocq, Hicks, *et al.*, 2020; Poli *et al.*, 2020; Xiao *et al.*, 2020). Many countries carried out lockdown measures to mitigate the COVID-19 pandemic. The government of Singapore implemented the nationwide partial lockdown or the so-called circuit breaker (CB) measures on 7 April 2020. The CB period lasted about two months, during which all nonessential workplaces were closed and all schools were transitioned to home-based learning. After CB ended, three-phase approach has been adopted to resume activities safely. Phase one (safe reopening) started on 2 June 2020, during which more people were allowed to go back to work and very few students were allowed to go to school. Phase two (safe transition) started on 19 June 2020, during which most business were allowed to resume and schools reopened at the end of June. Phase three (safe nation) started on 28 December 2020. According to Senior Minister of State for Health Janil Puthucheary, phase three would be a "new normal" that could last for a couple of years.

The lockdown measurements influence human activities significantly and lead to reduction in seismic vibrations above 1 Hz (Díaz *et al.*, 2017). Changes in seismic-noise levels have

been reported at global scale (Lecocq, Hicks, *et al.*, 2020), regional scale (Ojeda and Ruiz, 2020; Pérez-Campos *et al.*, 2020; Poli *et al.*, 2020; Somala, 2020; Xiao *et al.*, 2020; Yabe *et al.*, 2020; Cannata *et al.*, 2021; De Plaen *et al.*, 2021; Díaz *et al.*, 2021), and local scale (Lindsey *et al.*, 2020; Shen and Zhu, 2021; Wu *et al.*, 2021). Most of these studies assessed the overall seismic noise level changes over time based on averaged seismic amplitudes. Very few studies (Lindsey *et al.*, 2020) analyzed the interpretable information in seismic data for specific human activities such as traffic volume change as a result of lockdown. Recent fast-growing studies in urban geophysics suggest that human activities can be identified from the data recorded by traditional seismic sensors (e.g., Dean and Al Hasani, 2020; Fang *et al.*, 2020) and distributed acoustic sensing (Jakkampudi *et al.*, 2020; Lindsey *et al.*, 2020; Zhu *et al.*, 2021). To monitor the foot traffic volume of the runners, we deployed a seismic sensors in the West Coast Park in Singapore to monitor the lockdown effect on human running activities.

1. Department of Civil and Environmental Engineering, National University of Singapore, Singapore, Singapore,  <https://orcid.org/0000-0002-6573-7551> (YZ);  <https://orcid.org/0000-0001-9762-1548> (EN);  <https://orcid.org/0000-0003-3132-0085> (GF); 2. Department of Earth, Atmospheric, and Planetary Sciences, Purdue University, West Lafayette, Indiana, U.S.A.

\*Corresponding author: elita.li@nus.edu.sg

© Seismological Society of America

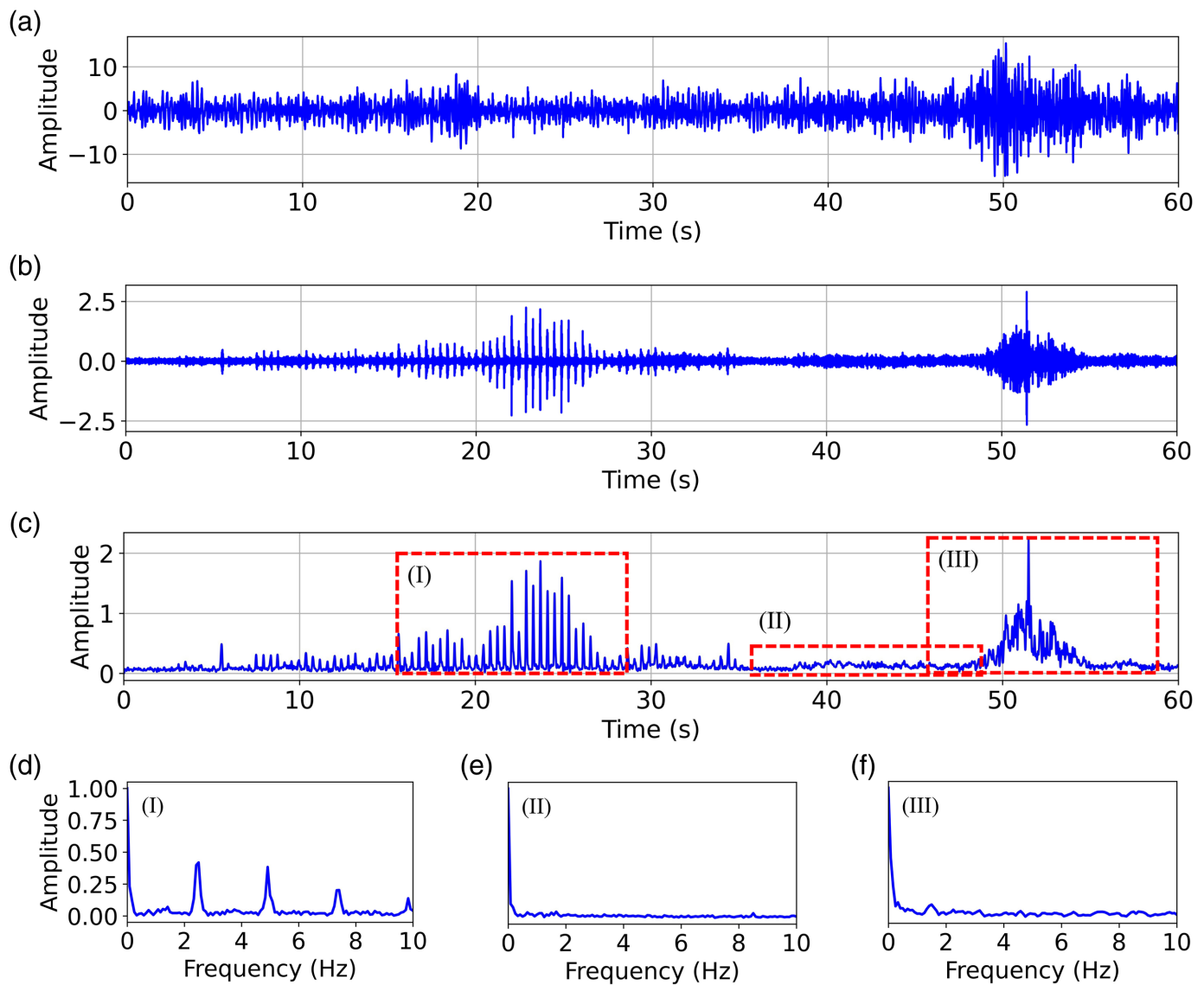
Human footsteps have been widely studied for the rich information they carry, not only about the individuals, but also about the surrounding environment and their interactions. Automatic footstep detection has been applied for indoor applications in fall detection (Clemente, Song, et al., 2019), patient monitoring (Pan et al., 2015), individual physical and emotional health evaluation (Li et al., 2019), indoor surveillance (Subramanian et al., 2009), customer behavior analysis (Pan et al., 2015), as well as providing occupancy, crowd dynamics, and human flow information (Tang et al., 2017). Footstep events are easily detected from preprocessed time-domain seismic vibration data recorded indoor according to their periodic and spiky features. Pan et al. (2014, 2015) extracted the step events (SEs) using an anomaly detection method in which an SE is detected if the sum of the squared values within a small window is beyond three standard deviations above the mean of the modeled Gaussian noise. Tang et al. (2017) separated the footstep signals from the background noise using an energy-threshold-based method in which footstep signals can be extracted if the maximum energy among the sensor array is larger than a dynamically updated threshold based on the distribution of Gaussian noise. Li et al. (2019) adopted the short-time average over long-time average (STA/LTA) method (Allen, 1978) to detect the footstep signals. The STA/LTA method calculates the ratio between the average absolute values of the amplitude in the consecutive moving short- and long-term windows. If the ratio exceeds a given threshold, an SE is identified. However, there are two main limitations of the STA/LTA method. One is that it is tricky to select appropriate trigger threshold and two window lengths (both short- and long-term windows). The other one is that STA/LTA only works well when the signal-to-noise ratio (SNR) of the data is high. Clemente, Li, et al. (2019) applied the S/L-Kurt Algorithm (Li et al., 2014) to extract the footstep signals as well as fall down vibrations.

For outdoor footstep applications such as outdoor surveillance (Houston and McGaffigan, 2003; Pakhomov et al., 2003; Park et al., 2008; Koç and Yegin, 2013; Anghelescu et al., 2015; Mukhopadhyay et al., 2017), an automatic footstep detection methods for seismic data recorded in a relatively quiet outdoor environment are similar to those in an indoor environment. The impulsive and periodic footstep features can also be extracted using time-domain methods. Kurtosis (Succi et al., 2001) is a statistical method based on the amplitude distribution of the vibration signals within a short-time window. Footstep signals can be detected with higher Kurtosis due to their spiky signatures than motor vehicles and background noise. Lacombe et al. (2006) and Anghelescu et al. (2015) detected the footstep signals by first calculating the kurtosis from the seismic data and then calculating the cadences to further determine if the signals are footstep signals. Koç and Yegin (2013) proposed a slow and quick adaptive thresholds algorithm to identify footsteps and vehicles. Time-domain footstep

detection methods are easy to implement and efficient. However, they rely heavily on the large footstep amplitudes compared to the ambient noise and often fail to identify or misidentify footsteps when the SNR of the footstep signals is low. Time-frequency methods, on the other hand, not only capture the nonstationary characteristic of the signals, but also partially remove the noise in the data. Xing et al. (2007) proposed an singular value decomposition-based adaptive threshold denoising algorithm in wavelet domain to remove the noise in the seismic data, and then detected the footstep signals base on the wavelet energy. However, they did not discuss if the method can distinguish footstep signals from high-energy vibration generated by motor vehicles in an urban outdoor environment.

Houston and McGaffigan (2003) proposed a spectrum analysis method to detect the footstep signals from the spectrogram of the band-pass filtered and downsampled envelope of seismic signals. Footsteps are then identified by verifying the value and SNR of primary frequency as well as second or third harmonic. The basic principle of the spectrum analysis method (Houston and McGaffigan, 2003) is illustrated in Figure 1. Figure 1a shows a 1 min raw data, Figure 1b is the filtered data obtained using a 40–100 Hz band-pass filter, and Figure 1c is the envelope of Figure 1b. Figure 1d–f shows the normalized spectrum obtained from the footstep signals, background noise, and signals generated by motor vehicles, respectively. There are three clear spikes in the spectrum of the footstep signals besides the 0 Hz peak and they are harmonics. However, in Figure 1e,f, the spectra are relatively flat and the energy is low beyond 0 Hz. With these different characteristics, Houston and McGaffigan (2003) identify strong footstep signals whose primary amplitude is above 11 dB SNR and the harmonic above 7 dB from seismic data recorded 40 m away from the road.

In the complex urban environments, however, footstep signals can be very noisy due to the high-level ambient noise coming from various kinds of natural and anthropological activities. The seismometer we use to record data in the West Coast Park in Singapore is about 5 m to the footway in the park and about 7 m to the Harbour Drive (Fig. 2). Large volume of motor vehicles enter and leave the 24-hr Parsar Panjang port terminal (Li et al., 2020). As a result, strong noise generated by the motor vehicles were continuously recorded in the data. These strong near-field traffic noise may bury the footstep signals (Fig. 3a). About 1.8 km northeast to the sensor, there is the West Coast Highway. The motor vehicles running on the highway also contribute to the low-frequency part of the data. Besides, frequent thunderstorms in Singapore resulted in high-energy spiky signals in the recorded data (Fig. 3b). These spiky signals are not acoustic signals but direct impacts of the raindrops falling on the imposed surface of the seismic sensor. We refer to these spiky signals as raindrop signals in this article. Thus, the algorithm proposed by Houston and McGaffigan (2003) is insufficient to detect the footstep signals from other overlapping signals. Following the same workflow



of Figure 1, Figure 3e shows an example in which weak footsteps cannot be identified, whereas Figure 3f shows an example in which raindrop signals may be misidentified. To overcome these challenges, we adapt the spectrum analysis method proposed by Houston and McGaffigan (2003) to achieve the following aims:

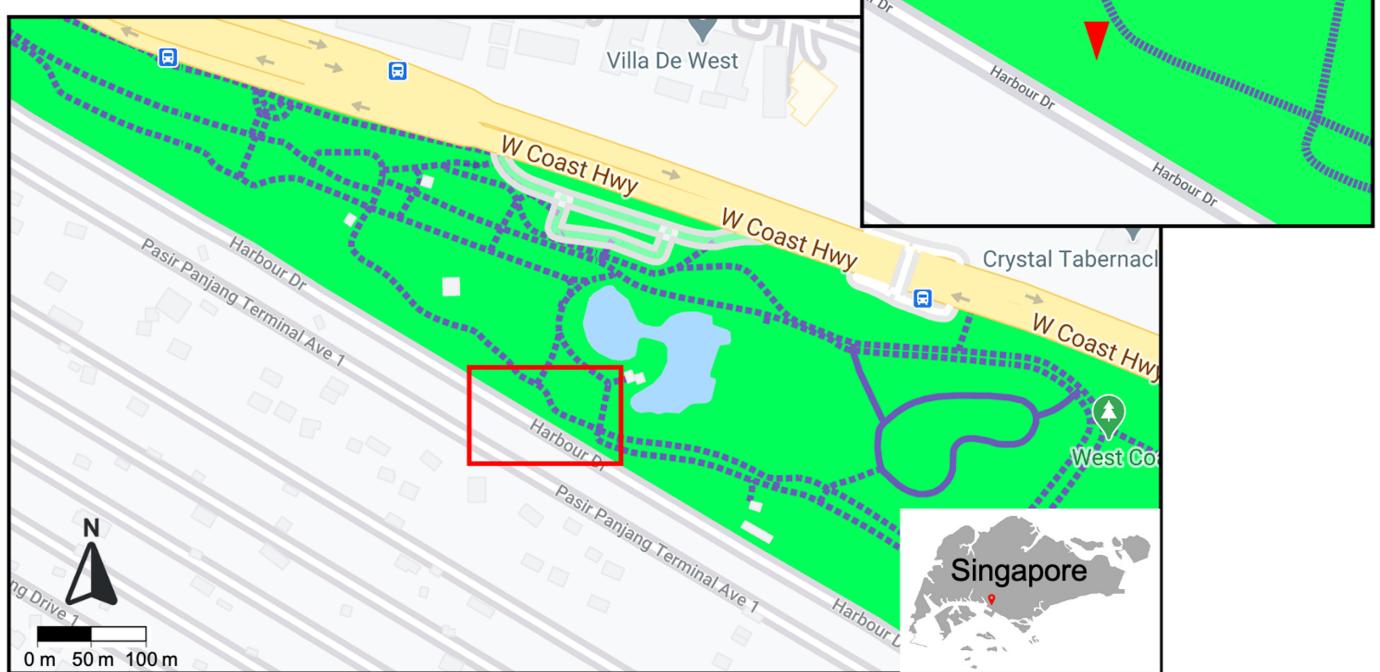
1. To provide accurate identification of footstep signals with low SNR.
2. To provide automatic processing for long-term monitoring of runner activities in urban environments.

The organization of this article is as follows. First, we discuss the modified runner identification algorithm in detail. Then, we provide hourly runner activity monitoring results obtained from four-month long monitoring seismic data. Next, we discuss the performance of the modified algorithm. Finally, we draw some conclusions in the last section.

**Figure 1.** Basic principle of footstep detection using the spectrum analysis method proposed by Houston and McGaffigan (2003): (a) 1 min raw data, (b) filtered data after applying a 40–100 Hz band-pass filter, (c) envelope of the band-pass filtered data displayed in (b), (d), (e), and (f) represents the normalized spectrum obtained from the footstep signal (labeled by the red dashed box in (c) with number (I)), background noise (labeled by the red dashed box in (c) with number (II)) and traffic noise generated by motor vehicles (labeled by the red dashed box in (c) with number (III)), respectively. The color version of this figure is available only in the electronic edition.

## Methodology

Runner detection consists of two tasks: footstep detection and runner counting. Our proposed algorithm first delineates footstep signals in each 3 s recording of vibrations induced by both natural and human activities. Multiple footstep detections within 12 s are counted as one runner based on the duration



statistics of a single running event on the seismic data. We use the  $N$ -component of the seismic recordings as it offers the best SNR for footstep signals.

The runner detection algorithm is summarized in Table 1. In this section, we give a detailed description for data preprocessing, detection, and counting. We introduce the tunable parameters for the proposed algorithm in each step and summarize them in Table 2.

### Data preprocessing

We take the preprocessing step to select the portions of seismic recordings that are more likely to contain footstep signals. As shown in Figure 1b, footstep signals are most prominent after bandpass between 40 and 100 Hz. Nonetheless, they are not the only signals that sit in this frequency band (Fig. 3a,b). Figure 4a–c shows the normalized spectrum obtained from band-pass filtered footstep signals (Movie S1, available in the supplemental material to this article), near-field traffic noise generated by motor vehicles (Movie S2), and spiky signals generated by raindrops (Movie S3), respectively. Consistent with the spectrograms displayed in movies S1–S3, the spectrum generated by the raindrop signals (Fig. 4c) has much higher energy at higher frequencies (80–100 Hz) compared to the other two. Thus, if the mean of the normalized amplitude from  $hf_l$  to  $hf_h$  is larger than 20% of the maximum amplitude, the signal is identified as generated by raindrops and discarded for further analysis. Otherwise, we calculate the envelope of the band-pass filtered data and corresponding normalized spectrum in each 3 s time window.

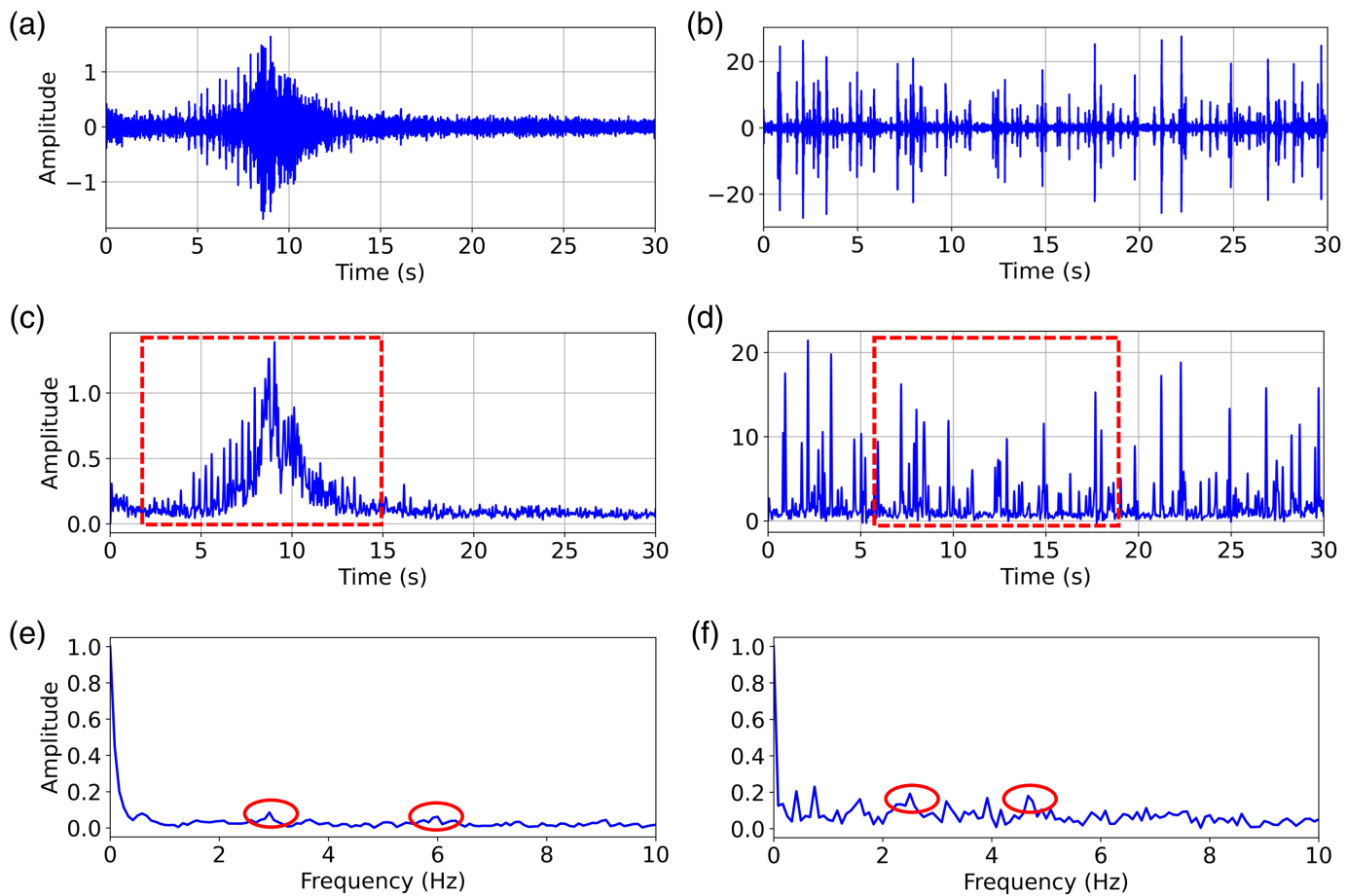
**Figure 2.** Map view of the site location. The site is located at the West Coast Park in Singapore, which is indicated by the red pinpoint in the map of Singapore in the lower right corner of this Figure. The red triangular represents the SmartSolo node we have used to record the data. The color version of this figure is available only in the electronic edition.

### Footstep detection

The detection criteria are: (a) the normalized spectrum obtained from the 3 s low-pass filtered envelope should have a strong primary. It should be larger than a predefined threshold  $a_p$ ; (b) the primary frequency  $pf$  should be in the frequency band  $pf_{\min}$  to  $pf_{\max}$ ; (c) the second harmonic should exist in the normalized amplitude spectrum. The frequency of the second harmonic  $sf$  should satisfy the constraint  $2 - \varepsilon < pf/sf < 2 + \varepsilon$ , in which  $\varepsilon$  represents how much  $pf/sf$  deviates from 2 and it results from the noise in the data. In the field data example, we assign  $a_p = 0.13$ . Because the cadence frequency of human footsteps is in the frequency band of 1–4 Hz (Mouring, 1994) and the typical walking range is between 0.6 and 2 Hz (Kang *et al.*, 2018), we set  $pf_{\min}$  and  $pf_{\max}$  as 2 Hz and 4 Hz, respectively. Finally, we choose  $\varepsilon$  as 0.2, which means we allow  $sf/pf$  to have a 20% deviation due to the noise from other sources in the data. With these criteria and parameters, we separate footsteps signals (Fig. 1a) from background ambient noise (Fig. 1b) and motor vehicles (Fig. 1c).

### Runner counting

We use a single-digit binary label to denote the footstep detection in each 3 s window. Our observation shows that runners



on average generate detectable seismic signals that last for 12 s. This time duration could change according to the particular site condition such as the distance between the footpath and the seismometer. Therefore, for each new detection of footprint, we assume that the subsequent 9 s of data record the signals from the same runner. When a single runner is identified, the peak frequency of his/her footprint signals is recorded to calculate the cadence as follows:

$$\text{cadence} = 60pf. \quad (1)$$

Figure 5 illustrates how the algorithm detects the footprint signals and counts the runners and their cadences. Figure 5a shows two challenging cases when the SNR is extremely low. The first case involves overlapping footsteps and a motor vehicle with  $\text{SNR} = -0.29 \text{ dB}$ , whereas the second case highlights a soft step signal in ambient noise with  $\text{SNR} = 0.52 \text{ dB}$ . Figure 5b is the envelope of Figure 5a. Figure 5c,d is the normalized spectrum obtained from the signals marked by the two red dashed boxes, respectively. The strong primary and second harmonic (marked by the red ellipses) are used to identify as the footprint signals. Thus, the corresponding segments are labeled to 1 (Fig. 5e). Figure 5f,g shows the corresponding runner counting vector and the cadence vector, respectively. In this 1 min recording, the algorithm detects two runners in total.

**Figure 3.** (a) 30 s data contains overlapping signals after 40–100 Hz band-pass filtering, (c) envelope obtained from (a), and (e) normalized spectrum obtained from the footprint signals marked by the red dashed box in (c). (b), (d), and (f) are the same as (a), (c), and (e), except for the signals in (b) are mainly generated by raindrops. The two harmonics in (e) and (f) are labeled by two red ellipses, respectively. The color version of this figure is available only in the electronic edition.

## Long-Term Runner Activity Monitoring

On 7 April 2020, the first day of CB in Singapore, we deployed a seismic sensor to record the footprint signals generated by runners in the West Coast Park. The seismic sensor we used to record the data is SmartSolo IGU-16HR 3C with 5 Hz corner frequency. The temporal sampling of the sensor can be up to 0.25 ms and it may attain reliable ambient noise data down to 0.2 Hz. The sampling rate of our recorded seismic data is 500 Hz. During data acquisition, the seismic sensor is replaced for recharging each month. We process all the data recorded from 7 April to 30 August and count the runners, together with their corresponding cadences in each hour each day. Figure 6a,b shows the average runner numbers in each hour from Monday to Sunday over the weeks during and after CB, respectively. There were two peaks of runner activities, one in the morning from 7:00 a.m. to 8:00 a.m., and the other

TABLE 1  
**Automatic Runner and Cadence Identification**

Algorithm 1 Automatic runner and cadence identification

**Input:**

raw data:  $d(t)$ , with length  $t_a$   
parameters:  $t_w, nt_w, f_{\min}, f_{\max}, hf_l, hf_h, a_{mn}, pf_{\min}, pf_{\max}, \varepsilon, a_p$

**Output**

runner numbers:  $r_{\text{num}}$

cadence of each runner:  $\mathbf{C}$ , with length  $r_{\text{num}}$

**Initialization:**

$\mathbf{C} \leftarrow \emptyset$   
 $r_{\text{num}} \leftarrow 0, label \leftarrow 0$

$N \leftarrow t_a \% t_w$

$i \leftarrow 0$

**Preprocessing:**

Bandpass filtering:  $d_{\text{bp}}(t) = f(d(t)) \leftarrow [f_{\min}, f_{\max}]$

Reshape:  $d_{\text{bp}}(t_w, N) \leftarrow d_{\text{bp}}(t)$

Calculate the spectrum of each column in  $d_{\text{bp}}(t_w, N)$  and then normalize with maximum amplitude:

$D \leftarrow \mathcal{F}(d(t_w, N)) / \max(\mathcal{F}(d(t_w, N)))$

Calculate the mean of each column in  $D$  in the frequency band  $[hf_l, hf_h]$ :

$A \leftarrow \text{mean}(|D[hf_l, hf_h]|)$

Calculate the envelope of  $d(t_w, N)$ :

$d_e \leftarrow \text{env}(d(t_w, N))$

Calculate spectrum of  $d_e$  and normalize with maximum amplitude:

$D_e = \mathcal{F}(d_e) / \max(\mathcal{F}(d_e))$

**Identification:**

**while**  $i < N$  **do**

**if**  $A(i) < a_{mn}$  **then**

Compute  $pf, sf$  using the  $i$ th trace of  $D$

**if**  $(pf_{\min} < pf < pf_{\max}) \&$  **then**

$(2 - \varepsilon < sf/pf < 2 + \varepsilon) \&$

$(D_{lf}(pf) > a_p)$

$label(i) = 1$

$c \leftarrow pf * 60$

append  $c$  to  $\mathbf{C}$

$r_{\text{num}} +=$

$i += nt_w$

**else:**

(Continued in next column.)

TABLE 1 (continued)  
**Automatic Runner and Cadence Identification**

```

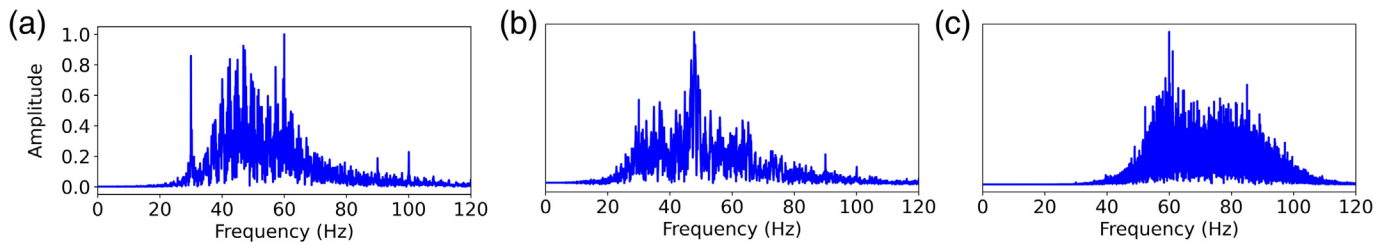
i ++
end if
else:
i ++
end if
end while

```

in the evening from 18:00 p.m. to 19:00 p.m. Almost no one ran at noon due to the tropical weather in Singapore. Runner activities during and after CB, were relatively stable in the morning, whereas runner activities in the evening decreased significantly as soon as CB ended, especially on weekends. Runner activities maintain a stable weekly cycle during and after CB, with constantly more runners over the weekends than during the work days. Nonetheless, the runner count shows that the preferred workout time over the weekend has changed according to the mitigation measures. During CB, the largest number of runners work out on Sunday evenings. After CB, the peak running hours are shifted to Saturday evenings. This suggests a heavy psychological stress that a normal working week places on urban residents.

TABLE 2  
**Parameters in Algorithm 1**

Parameter Types	Parameter	Value	Determining Factor
Preprocessing parameter	$t_w$	3 s	Temporal resolution
	$nt_w$	4	Footpath-seismometer distance
	$f_{\min}$	40 Hz	Sampling rate, footpath-seismometer distance
Raindrop parameter	$f_{\max}$	100 Hz	Sampling rate, footpath-seismometer distance
	$hf_l$	80 Hz	Sampling rate, rain rate intensity
Footstep parameter	$hf_h$	100 Hz	Sampling rate, rain rate intensity
	$a_{mn}$	0.2	Size of raindrops
Environment parameter	$pf_{\min}$	2 Hz	Minimum cadence of runner
	$pf_{\max}$	4 Hz	Maximum cadence of runner
$\varepsilon$	$\varepsilon$	0.2	Environment noise level
	$a_p$	0.13	Environment noise level



We collect the cadence data of the runners both for the morning runners (from 6:00 a.m. to 12:00 p.m.) and the evening runners (from 16:00 p.m. to 22:00 p.m.), and show the corresponding cadence statistics in Figure 7a,b, respectively. The most common cadences are 160 steps/min and 180 steps/min. We assume that runners paced at 180 steps/min and above are fast, professional-equivalent runners

(Dreyer and Dreyer, 2009; Daniels, 2013) and compare the percentage of fast runners in the morning and in the evening (Fig. 8). This observation suggests that people running in the weekday morning have higher cadence on average than those running in the evening. Although the evening runners with high cadences stayed relatively stable during the four-month period, morning runners with high cadences fell by about 5%. The blue curves denote the change of rainfall (in millimeters) at a nearby location in the morning (Fig. 7a) and evening (Fig. 7b) over time, respectively. We can observe the reduction in runner numbers on rainy days, which demonstrate that our algorithm performs well on eliminating the raindrop signals.

## Discussion

Global quieting of the low frequency (4–14 Hz) (Lecocq, Hicks, et al., 2020) seismic noise has been observed due to the lockdown measurements in major cities, due to the overall reduction of human traffic, construction, and other activities. However, the high-frequency band (40–100 Hz) seismic noise is more localized. In our case, it

**Figure 4.** Normalized spectrum obtained from the data after 40–100 Hz band-pass filtering: (a) footstep signals, (b) near-field traffic noise, and (c) raindrop signals. The color version of this figure is available only in the electronic edition.

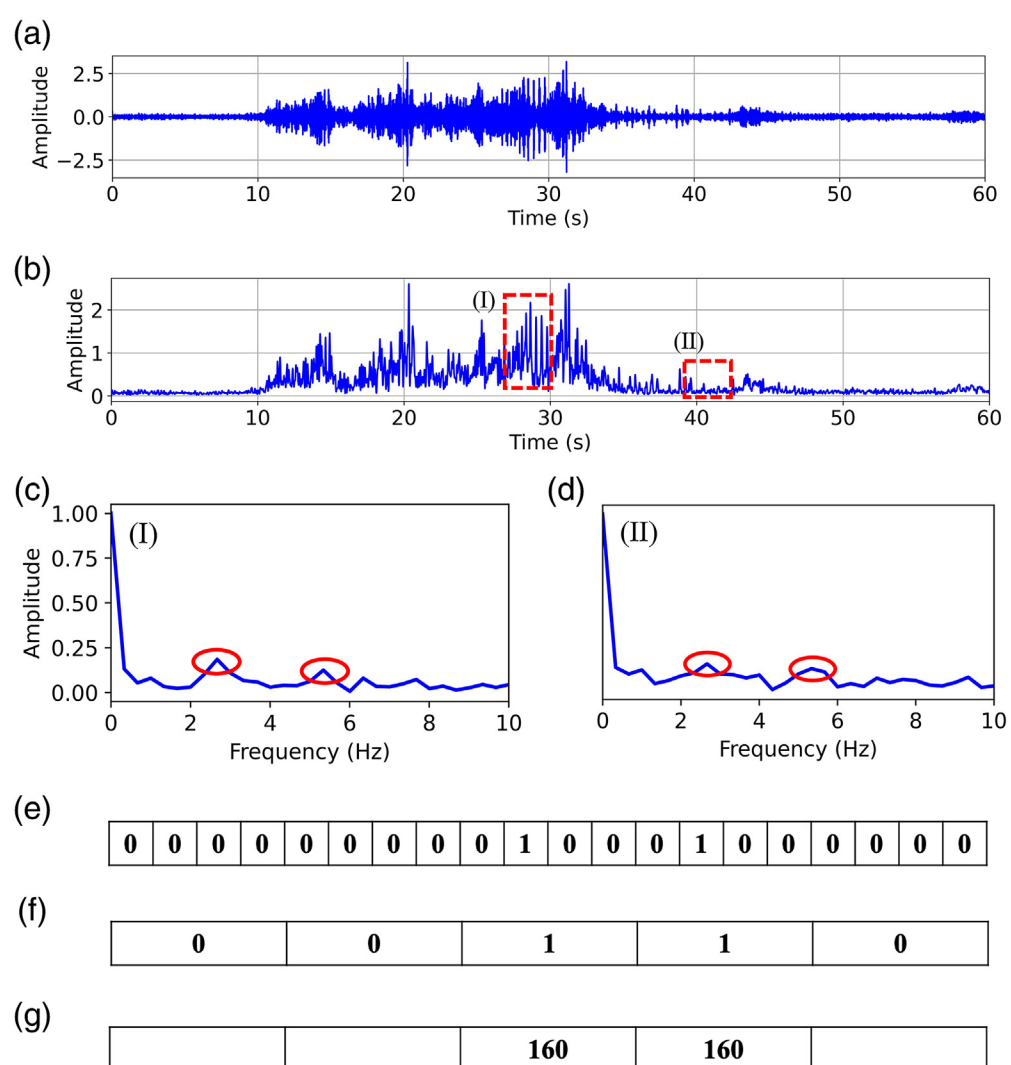


**Figure 5.** (a) 1 min data contains overlapping and weak footstep signals after 40–100 Hz band-pass filtering, (b) envelope obtained from (a), (c) and (d) are the normalized spectra obtained from the footstep signals marked by the red dashed boxes in (b) and the two maximum peaks are marked by the two red ellipses, (e) denotes the vector label corresponding to the data displayed in (a), (f) represents the runner numbers for each 12 s data, and (g) contains the cadences of the identified runners. The color version of this figure is available only in the electronic edition.

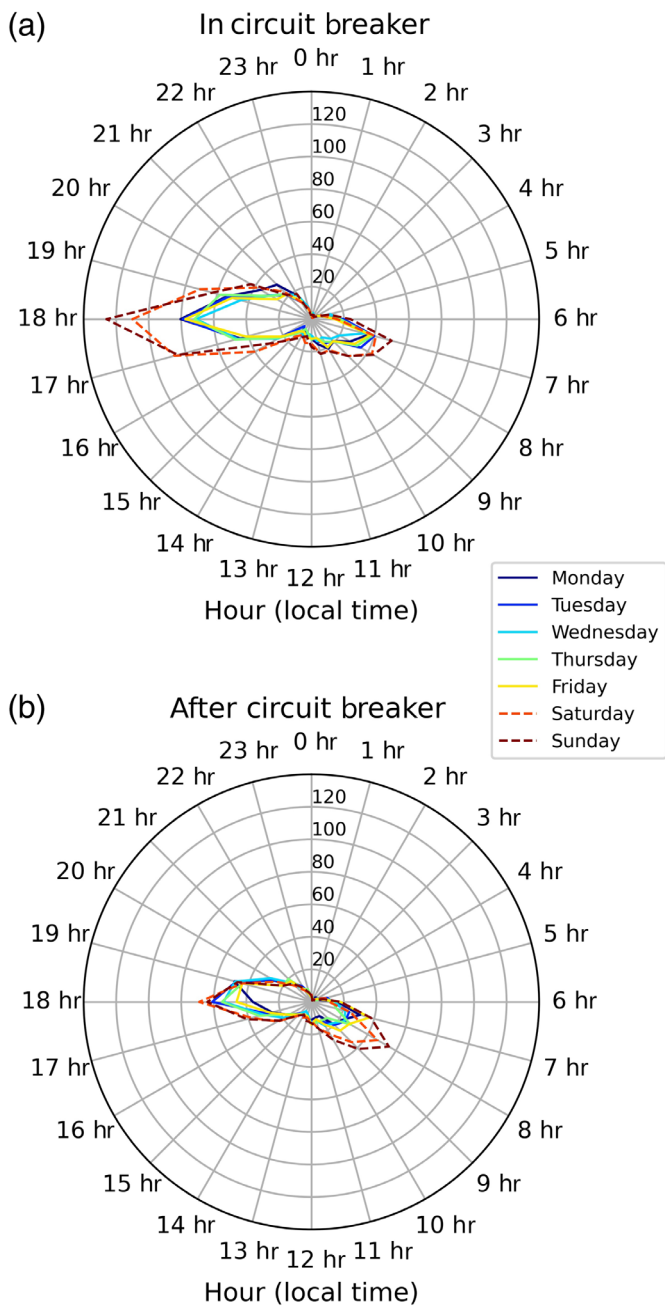


**Figure 6.** (a) Averaged runner numbers in each hour from Monday to Sunday over the weeks in the circuit breaker (CB), and (b) after CB. The color version of this figure is available only in the electronic edition.

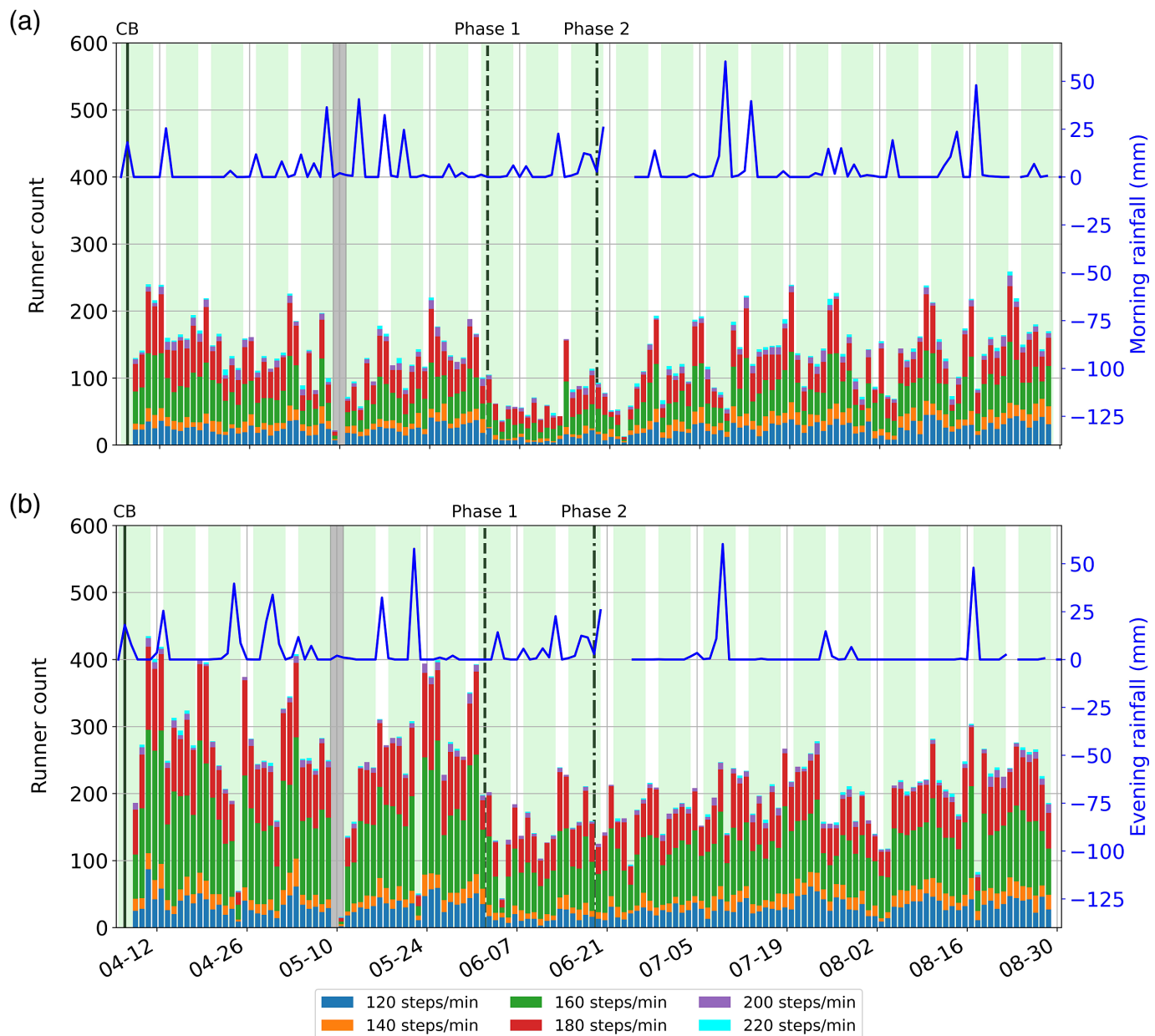
is determined by the traffic volume on the nearby road, which has seen constant traffic flow of heavy trucks because it connects the container port terminal with the city. As the container port terminal, an essential workplace, remained open 24/7 during CB, we have not observed much change in the high-frequency energy and the traffic volume (Li *et al.*, 2020). A similar finding was also reported by another study (Wu *et al.*, 2021). Lockdown measurements did not make it easier for us to detect weak

footstep signals from our recorded seismic data. Rather, our study demonstrates the robustness of the adapted algorithm against environmental noise.

The adapted algorithm performs well on distinguishing footstep signals from noise generated by other sources. The open-source codes we provide are very efficient. It takes less than 2 min to read and process one-day long seismic data from a network attached storage device where all data are stored. If data are streamed from the seismic stations to a cloud processing center via wireless network in the future, our algorithm can load data in shorter segments (on the order of minutes) and process the data nearly in real time. Because the algorithm is computationally efficient, it can also be potentially implemented as part of the firmware on the seismic station for edge computing. Thus, the size of information that requires real-time transmission can be dramatically reduced.

When counting the runners using the adapted algorithm, many parameters need to be carefully chosen. We list the parameters and their determining factors in Table 2. Preprocessing parameters including corner frequencies ( $f_{\min} = 40$  Hz,  $f_{\max} = 100$  Hz) of the band-pass filters, time-window length ( $t_w = 3$  s), and number of time-window length ( $nt_w = 4$ ) corresponding to a single runner duration (12 s) are primarily determined by the footpath-seismometer distance and should be tuned empirically for each site. Raindrop parameters including the corner frequencies ( $hf_l = 80$  Hz,  $hf_h = 100$  Hz) and the relative amplitude ratio ( $a_{mn} = 0.2$ ) are determined by the weather condition. The parameters used in this study are likely to be optimal for tropical environments, but should be adjusted where rain storms are less frequent and intense. Footstep parameters including bounds for primary frequency ( $pf_{\min} = 2$  Hz,  $pf_{\max} = 4$  Hz) are well established in sport science and do not need much adjustment. However, the parameters controlling footstep's relative strength to the environment noise ( $\sigma = 0.2$ ,  $a_p = 0.13$ ) should be adjusted. Our site is particularly noisy with a busy road less than 10 m away. Therefore, these parameters are chosen to be more tolerant. If data are acquired in more quiet sites, these parameters can be tightened. We use 3 s windows to detect the footstep signals, because we find empirically that this is the minimum window size that preserves the harmonics in the spectrum of footstep signals (Fig. S1). However, if we use a longer time window, the SNR of the signals in this window may be reduced since the footstep signals are easily contaminated by high-energy traffic noise in our seismic data. The temporal resolution of the algorithm is hence 3 s, which improves dramatically from tens of seconds (Houston and McGaffigan, 2003), and is sufficient for runner detection in the park. However, it might not be sufficient for occupancy detection in crowded indoor spaces such as malls and schools.

The results we have achieved in this article have an unprecedented resolution in space and time. Although large scale and low-frequency seismic responses of the whole urban space are interesting to observe, such localized, high-resolution



(meter-scale) observations have not been reported before. Monitoring runner density in parks during COVID-19 is very important, not only for mitigation measures to prevent virus spread, but also for the mental and physical health of urban residents. Although this might not be a classic seismological topic, extracting such rich information from seismic data for urban planning and management is a value-adding by-product of seismology. For example, based on the high human flow and occupancy at a recreational place obtained from the extracted footstep signals, a city planner may expand the space or upgrade the facilities to provide better service to urban residents. The extracted information may also be a good guidance for urban residents to plan their activities, such as not going to crowded places with high risk of infection of the virus. As we identified the raindrop signals from the seismic data, they can be used, for

**Figure 7.** (a) Cadences count of runners in the morning (from 6:00 a.m. to 12:00 p.m.) and (b) in the evening (from 16:00 p.m. to 22:00 p.m.) from 8 April to 30 August. In (a) and (b), the solid black line denotes the start of CB, whereas the black dashed and the dotted-dashed lines denote the start of phases 1 and 2 opening, respectively. Each bar contains several blocks that represent the cadences increasing from the bottom to the top. The blue curve displayed in (a) and (b) represent the rainfall (in millimeters) in the morning and evening, respectively. The color version of this figure is available only in the electronic edition.

example, to monitor the rainfall, which can be further used for weather forecast and water resource management. Apart from that, the traffic noise would contribute to low-cost, high efficiency and accuracy traffic monitoring in the urban environment

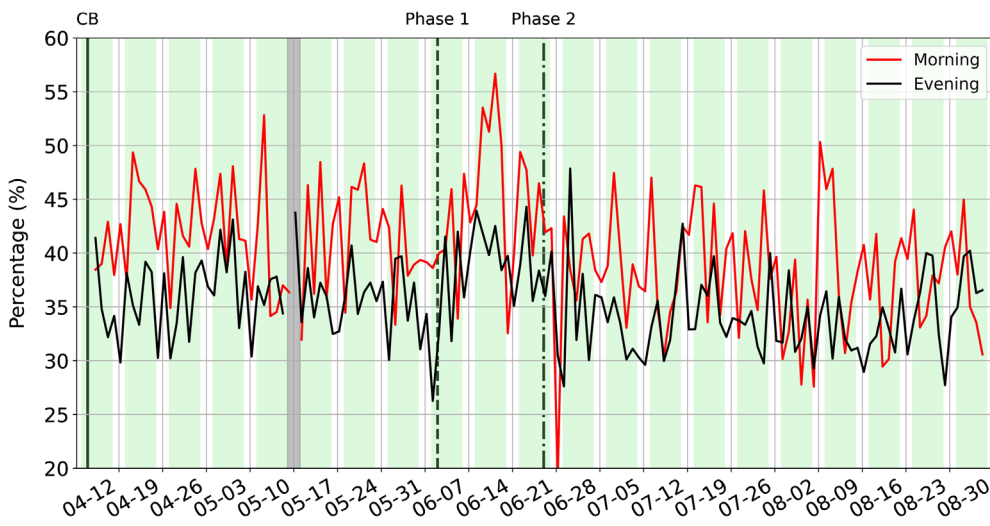


**Figure 8.** Percentage of runners with cadences above 180 steps/min in the morning (red curve) and in the evening (black curve) from 8 April to 30 August. The solid black line, the black dashed line, and the dotted-dashed line are the same as those in Figure 7. The color version of this figure is available only in the electronic edition.

(Ahmad and Tsuji, 2021). Finally, the method has the potential to contribute to traditional observational seismology. Human activities in urban areas usually contaminate the seismic recordings that are purposed for earthquake and/or other large-scale natural activities. Being able to identify and isolate the noise sources is the first step to remove such noise from the seismic data, for better observations of earthquakes and better understanding of the subsurface.

## Conclusions

In this article, we adapt the footstep detection algorithm proposed by Houston and McGaffigan (2003) and apply it to the seismic data recorded in an urban outdoor environment in Singapore during the COVID-19 pandemic. The adapted algorithm performs well in distinguishing the footstep signals from the signals generated by motor vehicles, frequent thunderstorms in Singapore, and the background noise. We demonstrate that the adapted algorithm identifies runners from overlapping and weak footstep signals and achieves a temporal resolution of 3 s. The highly efficient algorithm has the potential to process the data in real time and is suitable for long-term runner activity monitoring. Runner and cadence data in Singapore show that the COVID-19 pandemic encouraged more people to work out and runners statistically have higher cadence in the morning than in the evening. These results provide valuable information for residents who intend to workout for better health and performance.

## Data and Resources

Seismic data and the associate codes used in this study can be downloaded from <http://doi.org/10.5281/zenodo.4905734>. The seismic data

were read and processed with the open-source package Obspy (Krischer et al., 2015). All the figures except for Figure 2 were plotted using Matplotlib. Figures 6–8 were generated with the codes modified from the open-source package SeismoRMS kindly shared by Thomas Lecocq (Lecocq, Massin, et al., 2020). Figure 2 were generated from the Snazzy Maps website (<https://snazzymaps.com/>).

Information about the three phases after the circuit breaker (CB) in Singapore can be found from <https://www.gov.sg/article/ending-circuit-breaker-phased-approach-to-resuming-activities-safely>. The daily rainfall data were downloaded from <http://www.weather.gov.sg/climate-historical-daily/>. The morning and evening rainfall were obtained based on the daily rainfall and the hourly weather condition

on that day (<https://www.timeanddate.com/weather/singapore/singapore/historic>). Supplemental materials for this article include one figure in a word document and three movies. All websites were last accessed in August 2021.

## Declaration of Competing Interests

The authors acknowledge there are no conflicts of interest recorded.

## Acknowledgments

The authors acknowledge the Petroleum Engineering Professorship and Cambridge Sensing Pte Ltd. for its financial support of this research. The authors would like to thank editor Allison Bent, associate editor Brandon Schmandt, Nori Nakata, and two other anonymous reviewers for their constructive suggestions, which have been very helpful in improving the article.

## References

- Ahmad, A. B., and T. Tsuji (2021). Traffic monitoring system based on deep learning and seismometer data, *Appl. Sci.* **11**, 4590, doi: [10.3390/app11104590](https://doi.org/10.3390/app11104590).
- Allen, R. V. (1978). Automatic earthquake recognition and timing from single traces, *Bull. Seismol. Soc. Am.* **68**, 1521–1532.
- Anghelescu, P., G. V. Iana, and I. Tramandan (2015). Human footstep detection using seismic sensors, *2015 7th International Conf. on Electronics, Computers and Artificial Intelligence (ECAI)*, IEEE, Bucharest, Romania, 25–27 June 2015, AE-1, doi: [10.1109/ECAI.2015.7301179](https://doi.org/10.1109/ECAI.2015.7301179).
- Baldasano, J. M. (2020). COVID-19 lockdown effects on air quality by NO<sub>2</sub> in the cities of Barcelona and Madrid (Spain), *Sci. Total Environ.* **741**, 140353, doi: [10.1016/j.scitotenv.2020.140353](https://doi.org/10.1016/j.scitotenv.2020.140353).

- Baldwin, R. E., and B. Weder (2020). *Mitigating the COVID Economic Crisis: Act Fast and Do Whatever it Takes*, CEPR Press, London, United Kingdom, 8–9, available at <https://voxeu.org/content/mitigating-covid-economic-crisis-act-fast-and-do-whatever-it-takes> (last accessed September 2021).
- Bonaccorsi, G., F. Pierri, M. Cinelli, A. Flori, A. Galeazzi, F. Porcelli, A. L. Schmidt, C. M. Valensise, A. Scala, W. Quattrociocchi, et al. (2020). Economic and social consequences of human mobility restrictions under COVID-19, *Proc. Natl. Acad. Sci.* **117**, 15,530–15,535.
- Cannata, A., F. Cannavò, G. Di Grazia, M. Aliotta, C. Cassisi, R. S. De Plaen, S. Gresta, T. Lecocq, P. Montalto, and M. Sciotto (2021). Seismic evidence of the COVID-19 lockdown measures: A case study from eastern Sicily (Italy), *Solid Earth* **12**, 299–317.
- Clemente, J., F. Li, M. Valero, and W. Song (2019). Smart seismic sensing for indoor fall detection, location, and notification, *IEEE J. Biomed. Health Inf.* **24**, 524–532.
- Clemente, J., W. Song, M. Valero, F. Li, and X. Liy (2019). Indoor person identification and fall detection through non-intrusive floor seismic sensing, *2019 IEEE International Conf. on Smart Computing (SMARTCOMP)*, IEEE, 417–424, doi: [10.1109/SMARTCOMP500081](https://doi.org/10.1109/SMARTCOMP500081).
- Daniels, J. (2013). *Daniels' Running Formula*, Human Kinetics, Champaign, Illinois, 26–27.
- Dean, T., and M. A. Al Hasani (2020). Seismic noise in an urban environment, *The Leading Edge* **39**, 639–645.
- De Plaen, R. S., V. H. Márquez-Ramrez, X. Pérez-Campos, F. R. Zuñiga, Q. Rodrguez-Pérez, J. M. Gómez González, and L. Capra (2021). Seismic signature of the COVID-19 lockdown at the city scale: A case study with low-cost seismometers in the city of Querétaro, Mexico, *Solid Earth* **12**, 713–724.
- Díaz, J., M. Ruiz, and J.-A. Jara (2021). Seismic monitoring of urban activity in Barcelona during the COVID-19 lockdown, *Solid Earth* **12**, 725–739.
- Díaz, J., M. Ruiz, P. S. Sánchez-Pastor, and P. Romero (2017). Urban seismology: On the origin of earth vibrations within a city, *Sci. Rep.* **7**, 1–11.
- Dreyer, D., and K. Dreyer (2009). *Chirunning: A Revolutionary Approach to Effortless, Injury-Free Running*, Simon and Schuster, New York, New York, 111–112.
- Fang, G., Y. Elita Li, and O. Barak (2020). The seismic aircraft footprint: Probing near surface and tracking aircraft, *SEG Technical Program Expanded Abstracts 2020*, Society of Exploration Geophysicists, 2019–2023.
- Houston, K. M., and D. P. McGaffigan (2003). Spectrum analysis techniques for personnel detection using seismic sensors, *Unattended Ground Sensor Technologies and Applications V*, International Society for Optics and Photonics, 162–173, doi: [10.1117/12.500739](https://doi.org/10.1117/12.500739).
- Jakkampudi, S., J. Shen, W. Li, A. Dev, T. Zhu, and E. R. Martin (2020). Footstep detection in urban seismic data with a convolutional neural network, *The Leading Edge* **39**, 654–660.
- Kang, V., B. Huang, and G. Qi (2018). A novel walking detection and step counting algorithm using unconstrained smartphones, *Sensors* **18**, 297, doi: [10.3390/s18010297](https://doi.org/10.3390/s18010297).
- Koç, G., and K. Yegin (2013). Footstep and vehicle detection using slow and quick adaptive thresholds algorithm, *Int. J. Distr. Sensor Networks* **9**, 783604, doi: [10.1155/2013/783604](https://doi.org/10.1155/2013/783604).
- Krischer, L., T. Megies, R. Barsch, M. Beyreuther, T. Lecocq, C. Caudron, and J. Wassermann (2015). ObsPy: A bridge for seismology into the scientific Python ecosystem, *Comput. Sci. Discov.* **8**, 014003, doi: [10.1088/1749-4699/8/1/014003/meta](https://doi.org/10.1088/1749-4699/8/1/014003/meta).
- Lacombe, J., L. Peck, T. Anderson, and D. Fisk (2006). Seismic detection algorithm and sensor deployment recommendations for perimeter security, in *Unattended Ground, Sea, and Air Sensor Technologies and Applications VIII*, E. M. Carapezza (Editor), International Society for Optics and Photonics, Bellingham, Washington, 623109, doi: [10.1117/12.668766](https://doi.org/10.1117/12.668766).
- Lecocq, T., S. P. Hicks, K. Van Noten, K. Van Wijk, P. Koelemeijer, R. S. De Plaen, F. Massin, G. Hillers, R. E. Anthony, M.-T. Apoloner, et al. (2020). Global quieting of high-frequency seismic noise due to COVID-19 pandemic lockdown measures, *Science* **369**, 1338–1343.
- Lecocq, T., F. Massin, C. Satriano, M. Vanstone, and T. Megies (2020). SeismoRMS—A simple Python/Jupyter notebook package for studying seismic noise changes (1.0), Zenodo, doi: [10.5281/zenodo.3820046](https://doi.org/10.5281/zenodo.3820046).
- Li, F., J. Clemente, M. Valero, Z. Tse, S. Li, and W. Song (2019). Smart home monitoring system via footstep induced vibrations, *IEEE Syst. J.* **14**, no. 3, 3383–3389, doi: [10.1109/SYST.2019.2937960](https://doi.org/10.1109/SYST.2019.2937960).
- Li, F., J. Rich, K. J. Marfurt, and H. Zhou (2014). Automatic event detection on noisy microseismograms, *SEG Technical Program Expanded Abstracts 2014*, Society of Exploration Geophysicists, 2363–2367.
- Li, Y. E., E. Nilot, Y. Zhao, and G. Fang (2020). Seismology for urban activity monitoring in Singapore under the impact of COVID-19, *OSF Preprints*, doi: [10.31219/osf.io/tvj2w](https://doi.org/10.31219/osf.io/tvj2w).
- Lindsey, N. J., S. Yuan, A. Lellouch, L. Gualtieri, T. Lecocq, and B. Biondi (2020). City-scale dark fiber DAS measurements of infrastructure use during the COVID-19 pandemic, *Geophys. Res. Lett.* **47**, e2020GL089931, doi: [10.1029/2020GL089931](https://doi.org/10.1029/2020GL089931).
- Maliszewska, M., A. Mattoo, and D. Van Der Mensbrugghe (2020). The potential impact of COVID-19 on GDP and trade: A preliminary assessment, *World Bank Policy Research Working Paper No. 9211*, 10 April 2020, available at <https://ssrn.com/abstract=3573211> (last accessed September 2021).
- Mouring, S. E. (1994). Dynamic response of floor systems to building occupant activities, *Ph.D. Thesis*, The Johns Hopkins University, Maryland.
- Mukhopadhyay, B., S. Anchal, and S. Kar (2017). Detection of an intruder and prediction of his state of motion by using seismic sensor, *IEEE Sensors J.* **18**, 703–712.
- Ojeda, J., and S. Ruiz (2020). Seismic noise variability as an indicator of urban mobility during COVID-19 pandemic in Santiago metropolitan region, Chile, *Solid Earth Discuss.* **12**, 1–25, doi: [10.5194/se-12-1075-2021](https://doi.org/10.5194/se-12-1075-2021).
- Pakhomov, A., A. Sicignano, M. Sandy, and E. T. Goldburt (2003). Seismic footstep signal characterization, *Sensors, and Command, Control, Communications, and Intelligence (C3I) technologies for Homeland Defense and Law Enforcement II*, International Society for Optics and Photonics, 297–305, doi: [10.1117/12.487751](https://doi.org/10.1117/12.487751).
- Pan, S., A. Bonde, J. Jing, L. Zhang, P. Zhang, and H. Y. Noh (2014). BOES: Building occupancy estimation system using sparse ambient vibration monitoring, *Sensors and Smart Structures Technologies for Civil, Mechanical, and Aerospace Systems 2014*,

- International Society for Optics and Photonics, 90611O, doi: [10.1117/12.2046510](https://doi.org/10.1117/12.2046510).
- Pan, S., N. Wang, Y. Qian, I. Velibeyoglu, H. Y. Noh, and P. Zhang (2015). Indoor person identification through footstep induced structural vibration, *Proc. of the 16th International Workshop on Mobile Computing Systems and Applications*, 81–86, doi: [10.1145/2699343.2699364](https://doi.org/10.1145/2699343.2699364).
- Park, H. O., A. A. Dibazar, and T. W. Berger (2008). Protecting military perimeters from approaching human and vehicle using biologically realistic dynamic synapse neural network, *2008 IEEE Conf. on Technologies for Homeland Security*, IEEE, 73–78, doi: [10.1109/THS.2008.4534426](https://doi.org/10.1109/THS.2008.4534426).
- Pérez-Campos, X., V. H. Espndola, D. González-Ávila, B. Zanolli Fabila, V. H. Márquez-Ramrez, R. S. De Plaen, J. C. Montalvo-Arrieta, and L. Quintanar (2020). The effect of confinement due to COVID-19 on seismic noise in Mexico, *Solid Earth Discuss.* **12**, 1–14, doi: [10.5194/se-12-1411-2021](https://doi.org/10.5194/se-12-1411-2021).
- Poli, P., J. Boaga, I. Molinari, V. Cascone, and L. Boschi (2020). The 2020 coronavirus lockdown and seismic monitoring of anthropic activities in Northern Italy, *Sci. Rep.* **10**, 1–8.
- Shen, J., and T. Zhu (2021). Seismic noise recorded by telecommunication fiber optics reveal the impact of COVID-19 measures on human activities, *Earth and Space Science Open Archive ESSOAr*, doi: [10.1002/essoar.10504512.2](https://doi.org/10.1002/essoar.10504512.2).
- Sicard, P., A. De Marco, E. Agathokleous, Z. Feng, X. Xu, E. Paoletti, J. J. D. Rodriguez, and V. Calatayud (2020). Amplified ozone pollution in cities during the COVID-19 lockdown, *Sci. Total Environ.* **735**, 139542, doi: [10.1016/j.scitotenv.2020.139542](https://doi.org/10.1016/j.scitotenv.2020.139542).
- Somala, S. N. (2020). Seismic noise changes during COVID-19 pandemic: A case study of Shillong, India, *Nat. Hazards* **103**, 1623–1628.
- Subramanian, A., S. G. Iyengar, K. G. Mehrotra, C. K. Mohan, P. K. Varshney, and T. Damarla (2009). A data-driven personnel detection scheme for indoor surveillance using seismic sensors, *Unattended Ground, Sea, and Air Sensor Technologies and Applications XI*, International Society for Optics and Photonics, 733315, doi: [10.1117/12.820237](https://doi.org/10.1117/12.820237).
- Succi, G. P., D. Clapp, R. Gampert, and G. Prado (2001). Footstep detection and tracking, *Unattended Ground Sensor Technologies and Applications III*, International Society for Optics and Photonics, 22–29, doi: [10.1117/12.441277](https://doi.org/10.1117/12.441277).
- Tang, X., M.-C. Huang, and S. Mandal (2017). An “Internet of Ears” for crowd-aware smart buildings based on sparse sensor networks, *2017 IEEE Sensors*, IEEE, 1–3, doi: [10.1109/ICSENS.2017.8234263](https://doi.org/10.1109/ICSENS.2017.8234263).
- Wu, B., R. Douilly, H. A. Ford, G. Funning, H.-Y. Lee, S. Niyogi, M. Mendoza, C. Kyriakopoulos, and D. Oglesby (2021). Monitoring human activity at a very local scale with ground-motion records: The early stage of COVID-19 pandemic in California, USA, New York City, USA, and Mexicali, Mexico, *Seismol. Res. Lett.* **92**, no. 5, 3007–3023.
- Xiao, H., Z. C. Eilon, C. Ji, and T. Tanimoto (2020). COVID-19 societal response captured by seismic noise in China and Italy, *Seismol. Soc. Am.* **91**, 2757–2768.
- Xing, H.-F., F. Li, and Y.-L. Liu (2007). Wavelet denoising and feature extraction of seismic signal for footstep detection, *2007 International Conf. on Wavelet Analysis and Pattern Recognition*, IEEE, 218–223, doi: [10.1109/ICWAPR.2007.4420667](https://doi.org/10.1109/ICWAPR.2007.4420667).
- Yabe, S., K. Imanishi, and K. Nishida (2020). Two-step seismic noise reduction caused by COVID-19 induced reduction in social activity in metropolitan Tokyo, Japan, *Earth, Planet Space* **72**, 1–11.
- Zambrano-Monserrate, M. A., M. A. Ruano, and L. Sanchez-Alcalde (2020). Indirect effects of COVID-19 on the environment, *Sci. Total Environ.* **728**, 138813, doi: [10.1016/j.scitotenv.2020.138813](https://doi.org/10.1016/j.scitotenv.2020.138813).
- Zhu, T., J. Shen, and E. R. Martin (2021). Sensing Earth and environment dynamics by telecommunication fiber-optic sensors: An urban experiment in Pennsylvania, USA, *Solid Earth* **12**, 219–235.

---

Manuscript received 9 June 2021  
Published online 29 September 2021